



A simple method for determination of mercury (II) ions by PNBS-doped carbon dots as a fluorescent probe

Changiz Karami¹ · Mohammad Ali Taher² · Mohsen Shahlaei¹

Received: 3 November 2019 / Accepted: 21 February 2020 / Published online: 3 March 2020
© Springer Science+Business Media, LLC, part of Springer Nature 2020

Abstract

A simple and efficient fluorometric method is described for detecting mercury (II) ions. Carbon quantum dots doped with nitrogen, sulfur, phosphorus, and boron were prepared by a one-step hydrothermal method for first time that involves heating of a solution of glucose, thiourea, boric acid, and phosphoric acid in an autoclave simultaneously for 5 h at 200° C. The carbon quantum dots with phosphorus, sulfur, boron, and nitrogen atom (PNBS-CQDs) are a viable probe for fluorometric detection of Hg²⁺. Unlike CQD-based probes reported so far, the addition of Hg²⁺ causes a decrease in fluorescence signal (with excitation/emission maxima at 450/530 nm). The probe has a linear response in the 25.0 μM to 1500.0 mM of Hg²⁺ concentration range with 5.0 μM (S/N = 3) and 16.5 μM for LOD and LOQ, respectively. The developed method was successfully applied for determining the mercury (II) ions in real samples.

1 Introduction

In nature, there are a lot of chemicals that over a limit of its amount can be harmful to all of their living organisms such as heavy metals. The environmental pollution by heavy metals, especially in water, is a severe threat to the environment and public health since heavy metal ions are toxic and indissoluble and tend to accumulate in organisms [1]. One of the most studied heavy metals that cause serious health concern is mercury (II) ion [2]. Bacteria that live in aquatic sediments can convert mercury ions into methyl mercury, along with accumulating through the food chain in the human body and cause many brain diseases, and kidneys [3]. Mercury ion easily passes through the skin, respiratory, and gastrointestinal tissues, and damages DNA causing many problems, including permanent damage to the central nervous system [4, 5]. In recent years, extensive research has been done to develop new nanoparticles [6–12].

However, the design of a sensitive and selective method is important for measuring the amount of mercury (II) ion. Techniques such as polarography, Inductively coupled plasma mass spectrometry (ICP-MS), atomic absorption/emission spectroscopy, and Auger electron spectroscopy which were used for determining Hg require sophisticated instrumentation and/or complicated sample preparation that limits their applications [13–15]. Fluorescence nanoparticles have been highly attracted considerable attention for their specific abilities, and this is the reason for many fields such as chemistry, biology, and so on which myriad applications have been defined for them [16–18]. Semiconductor quantum dots are well-developed fluorescence nanoparticles compounds, but their applications are limited because of the release of heavy metals such as lead and cadmium, which cause environmental contamination [19]. Compounds such as silver nanoparticles and gold nanoparticles, which have fluorescence properties, have been studied on the basis of their excellent photostability and low toxicity [20]. However, the synthesis of these fluorescent nanoparticles requires expensive materials such as metal salts, DNA, proteins, peptides, thiol ligands, which limit their extensive preparation and further applications [21]. Therefore, the development of highly fluorescent nanoparticles with good photostability, low toxicity, and easy-to-synthesize is very tempting for researchers. Carbon quantum dots nanoparticles have gained great attention due to their easy fabrication, high quantum yield, low cost, low toxicity, excellent biocompatibility, and

✉ Changiz Karami
Changiz.karami@gmail.com

✉ Mohsen Shahlaei
mohsenshahlaei@yahoo.com

¹ Pharmaceutical Sciences Research Center, Health Institute, Kermanshah University of Medical Sciences, Kermanshah, Iran

² Department of Chemistry, Faculty of Sciences, Shahid Bahonar University of Kerman, Kerman, Iran

good photostability [22]. By the way, carbon quantum dots have been widely used in cell labeling, bio-imaging, and the identification of various compounds [23–26], and also has been specifically used to detect H_2O_2 [27, 28] and mercury (II) [29, 30]. Although CQDs that is introduced as a probe for different compounds may be very effective and useful, the design of new CQDs that can overcome constraints, as well as high fluorescence stability carbon nanoparticles, is required to fit the application fields.

The PBSN-CQDs with four heteroatoms were synthesized for the first time via hydrothermal method using the simple hydrothermal method and low-cost materials such as phosphoric acid, thiourea, glucose, and boric acid. The synthesized PBSN-CQDs were characterized by XRD, TEM, fluorescence spectrophotometer, UV–Vis, and FT-IR. PBSN-CQDs are introduced as probe for Hg^{2+} with different strategies which are associated with fluorescence "off" state. However, the mechanism for detecting mercury ions is different because PBSN-CQDs + Fe^{2+} is used as a probe for the detection of Hg^{2+} . Upon the addition of Hg^{2+} , Fe^{2+} was oxidized to Fe^{3+} and Hg^{2+} convert to Hg^0 in the acidic condition which triggers quenching. Nevertheless, it is possible to relate the amount of fluorescence quenching to the concentration of mercury ion. Furthermore, the specificity response to Hg^{2+} , the influence of other compounds on the PBSN-CQDs response was studied. The obtained functional PBSN-CQDs displayed enhanced sensitive response toward Hg^{2+} in 25.0–1500.0 μM concentration range with 5 min response time; additionally, its application for determining Hg^{2+} in the real sample was investigated. Futuristically, it will play an important role in enriching the detection methods for other harmful material and can be contributing to the development of the doped PBSN-CQD-based fluorescence probe (Scheme 1).

2 Experimental section

2.1 Materials

Phosphoric acid, thiourea, boric acid, and glucose were purchased from Sigma-Aldrich. Potassium dihydrogen phosphate (KH_2PO_4) and dipotassium hydrogen phosphate trihydrate ($\text{K}_2\text{HPO}_4 \cdot 3\text{H}_2\text{O}$) were acquired from Merck for

preparation of PB buffer solution. Other chemical compounds such as nitrate salt of silver (I), Manganese (II), lead (II), magnesium (II), manganese (II), iron (III), iron (II), cobalt (II), cadmium (II) and biological compounds—catechol, nitrite, glucose, L-cysteine, and hydrogen peroxide—were purchased from Merck Co. All chemicals were used with high purity and without further purification.

2.2 Characterization

The fluorescence spectra were recorded by an LS45 spectrometer (PerkinElmer, US). The fluorescence emission spectra of PBSN-CQDs were recorded from 460 to 600 nm with excitation wavelength at 450 nm at room temperature. The Cary 100 spectrometer was used for studying the optical properties. The transmission electron microscope (TEM) was used for measurement of particles size and obtained on a JEOL-JEM 2010 Transmission Electron Microscope (Japan) operated at 200 kV. AVATAR 370-IR spectrometer (Thermo Nicolet, USA) was used for FT-IR spectra recording in the wavenumber range 400–4000 cm^{-1} . X-ray powder diffraction (XRD) results were collected with a Rigaku Ultima IV XRD diffractometer (Rigaku, Japan) equipped with graphite monochromatized high-intensity Cu-K α radiation ($\lambda = 1.5417 \text{ \AA}$).

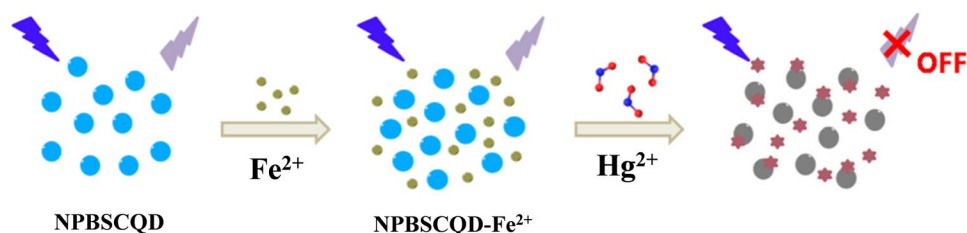
2.3 Hydrothermal synthesis of PBSN-CQDs

The PBSN-CQDs was synthesized by one-pot hydrothermal method. Briefly, 0.2 g of glucose, 0.2 g of boric acid, 0.2 g of thiourea, and 5 ml of phosphoric acid in 20 ml distilled water were dissolved. Then, the solution was transferred in the Teflon-line stainless steel autoclave at 200 °C for 5 h until the reaction was completed. After the autoclave was cooled to ambient temperature, a dark brown solution was obtained which was centrifuged at (10,000 rpm) for 10 min to remove the large and agglomerate particles. The suspension was filtered for removing the large dots. A brownish red PBSN-CQDs solution was finally obtained.

2.4 Detection of Hg^{2+} ion

At first, 100 μL of Fe^{2+} (0.01 M) were added to 50 μg of PBSN-CQDs and diluted up to 2 mL by a phosphate

Scheme 1 Schematic illustration of the detection process for Hg^{2+}



buffer (PBS, 0.1 M, pH 4). Then, the resulted solution was incubated at 25 °C. Next, different concentrations of Hg^{2+} ion (25.0–1500.0 μM) were added after the fluorescence stability was obtained at 5 min. The fluorescence spectrum is recorded under excitation at 450 nm. In the range of 25.0 μM to 1500.0 μM , the calibration plot is linear, and LOD was calculated with the signal to noise ratio ($S/N = 3$). For PBSN-CQDs selectivity, 150.0 μM of potential interferences such as metal ions (that are similar to Hg^{2+} ion) and biochemical compounds were added and examined.

2.5 Interference for detection of Hg^{2+} ion

The fluorescence response in the region of 530 nm of the mixture of PNBS-CQDs + Fe^{2+} (50 μg PNBS-CQDs and 100 $\mu\text{L} \times 0.01$ M of Fe^{2+}) in a solution containing 100 μM of mercury (II) and 2.0 mM of other compounds such as silver (I), lead (II), magnesium (II), manganese (II), iron (III), cobalt (II), cadmium (II), phenol, catechol, NO_2 , glucose, melamine, urea, thiourea, and L-cysteine is recorded separately in pH 4 and 25 °C.

2.6 Detection of Hg^{2+} ion in drinking water

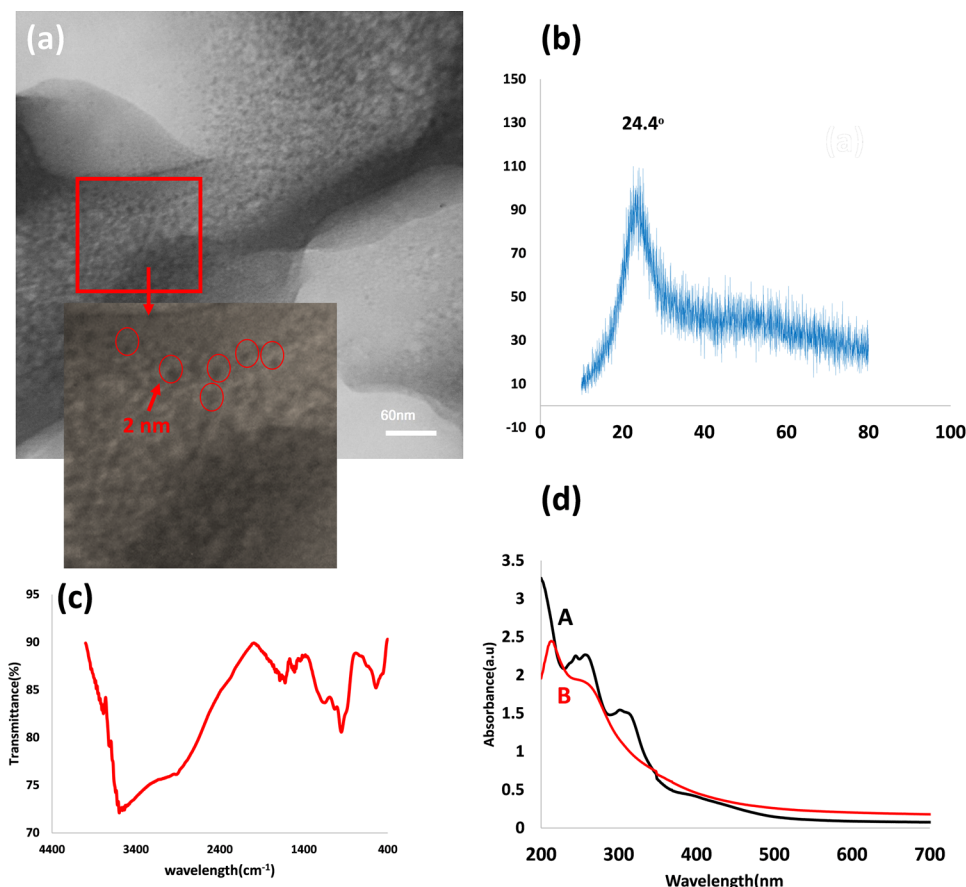
For evaluating the PBSN-CQDs + Fe^{2+} -based probe for Hg^{2+} detection in a real system, the performance of the developed method for real water sample analysis was examined by tap water and River water samples. The tap water samples were filtered through a 0.20 μm filtered membrane and then centrifuged at 10,000 rpm for 20 min. The resultant water samples were spiked with Hg^{2+} at different concentration and then analyzed with the proposed method.

3 Results and discussion

3.1 Characterization of PBSN-CQDs

Carbon quantum dots containing heteroatoms such as nitrogen, sulfur, boron, and phosphorus were prepared using a common and well-known hydrothermal method. The chemicals material that used for this structure was thiourea, boric acid, boron, phosphoric acid, and glucose. For the study of the particle size and morphology of the PBSN-CQDs, transmission electron microscopy (TEM) analysis was carried out. As shown in Fig. 1a, two results are obtained: first, the structure is spherical and second, the particle size is

Fig. 1 Characterization of PBSN-CQDs. **a** TEM micrograph of PBSN-CQDs. **b** XRD pattern of PBSN-CQDs. **c** UV–Vis absorption of PBSN-CQDs (curve A) and CQDs (curve B). **d** FT-IR transmitted spectra of PBSN-CQDs



approximately uniformly distributed, and the particle diameter is about 3 nm between about 30 nanoparticles that is shown in Fig. 1a. The next analysis is the XRD spectrum which is shown in Fig. 1b. Additionally, the broad peak at $2\theta = 24.3$ attributing to (002) peak of graphite indicates that CQDs were successfully synthesized, which relates to the structure of carbon amorphous and other materials such as oxygen and heteroatoms in this structure also being in good agreement with that described in literature [31]. To verify the functional groups on the surface of the PBSN-CQDs structure, FT-IR has been used. According to Fig. 1c, the index peaks found in 3420 cm^{-1} , which correspond to $-\text{OH}$. The peak 3213 cm^{-1} corresponds to $-\text{NH}$, and 2920 cm^{-1} corresponds to $-\text{C}=\text{C}-\text{H}$. The peaks related to $\text{C}-\text{H}$ and $-\text{SH}$ are in the region of 2850 and 2350 cm^{-1} , respectively. The peaks at 1667 cm^{-1} correspond to $-\text{C}=\text{O}$. The peaks at 1498 cm^{-1} and 1454 cm^{-1} corresponds to $-\text{C}=\text{C}$. The peaks which are seen at 1248 cm^{-1} relate to $\text{C}-\text{O}$. The peak of 1105 cm^{-1} corresponds to $-\text{CN}$, as well as the peaks seen in 515 to 759 cm^{-1} $-\text{CS}$ [32]. The peak of $\text{P}-\text{O}-\text{H}$ and $\text{P}=\text{O}$ are seen in 360 cm^{-1} and 1348 cm^{-1} , respectively [33–35]. And finally, to show the presence of a boron atom, it is sufficient to know the spectrum of 1405 cm^{-1} associated with the asymmetric vibrations of $\text{B}-\text{O}$, which indicates the presence of boron in the structure of PBSN-CQDs [36].

3.2 Investigation of optical properties

For investigating the PBSN-CQDs optical properties, the UV/Vis absorption spectra in an aqueous solution were studied. As shown in Fig. 1d, curve A an absorption band in the 285 nm region is related to the transition of $\pi-\pi^*$ in the $\text{C}=\text{C}$ band [32]. Two other absorption spectra in the area of 275 and 336 nm can be seen related to the transition of

$n-\sigma^*$ in the $\text{C}=\text{O}$ band and the surface defect is caused by heteroatoms such as nitrogen, phosphorus, and carbon [37, 38]. In the region of 302 and 370 nm , there are two absorption bands that are correspond to electron transfer of $n-\pi^*$ in the $\text{B}-\text{C}$ bond [39]. Compared to CQDs (Fig. 1d curve B) which have no heteroatom, the absorption peak can be seen only in the region of 260 nm that is related to the transfer of $\pi-\pi^*$ in the $\text{C}=\text{C}$ band and the transfer of $n-\sigma^*$ in the $\text{C}=\text{O}$ band. However, the fluorescence spectra were investigated at the different excitation wavelength (320 to 490 nm). As shown in Fig. 2a, at 320 nm to 370 nm excitation wavelength emission is broad, and there is no sharp and usable spectrum. With further increase in the excitation wavelength (370 to 490 nm), the emission intensity also increased. So, the excitation spectrum for PBSN-CQDs at 450 nm and the emission spectrum at 530 nm are studied [40].

3.3 Fluorescence stability of PBSN-CQDs

Since fluorescence is emitted from the surface of PBSN-CQDs as the optical properties, the study of the effect of different pH on the intensity of fluorescence is undoubtedly essential. Anyway, to find the best pH, the amount of $50\text{ }\mu\text{g}$ of PBSN-CQDs was added to 2 ml of different pH value, and the fluorescence intensities were recorded. As shown in Fig. 2b, the fluorescence intensity is the lowest in acidic pHs, and the fluorescence intensity increases as well until the pH ranges $6-8$. Also, in this range of pH, the amount of fluorescence intensity is constant without any obvious change in fluorescence intensity. The reason for the stability of fluorescence intensity during changing the pH is that the PNBS-CQDs are saturated with carbonyl and hydroxyl groups. Then, these functional groups are protected by acidic solutions when the mixture is in acidic environments,

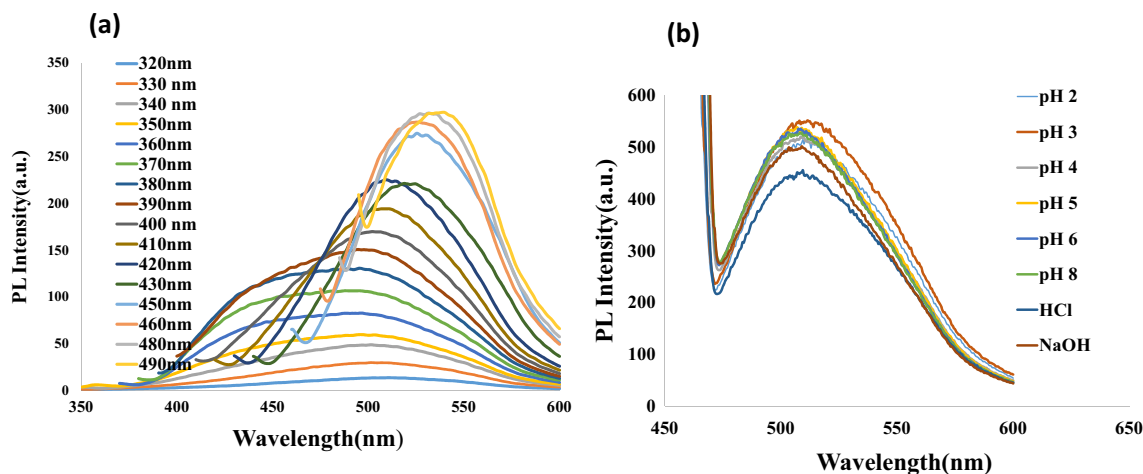


Fig. 2 **a** Fluorescence spectrum of the as-synthesized PBSN-CQDs at different excitation wavelength. **b** Fluorescence stability of PBSN-CQDs in different pH

causing aggregation of PNBS-CQDs and resulting in the fluorescence quenching [41].

3.4 Response mechanism for detecting mercury (II) ions

The synthesized PNBS-CQDs was used for determining mercury ions in aqueous medium. Based on the specific mechanism that is described, this probe is designed to detect mercury (II) ions. By the way, the electrons leaped into the excited state from the lowest energy level by excited and the electrons in this place are unstable so the electrons return to its ground state. The transmission of electrons leads to efficient energy transfer, so it produces the fluorescence. After adding of iron (II) ion to PNBS-CQDs, no significant change in the fluorescence intensity was observed. However, with the adding of mercury (II) ions to the PNBS-CQDs + Fe²⁺, the fluorescence intensity was changed that is due to the production of mercury (Hg_c⁰) according to Eq. (1, 2) [42].



When mercury (Hg_c⁰) are produced, accordingly, the latter provided the unfilled orbital for the electrons of PNBS-CQDs in the excited state, which resulted in a decrease or “quenching” of the fluorescence intensity. By this quenching effect, described above, and the oxidation principle, a quenching fluorescent probe for determination of Hg²⁺ ion was designed. According to Fig. 3, in the presence of iron (II), iron (III), and mercury (II) ions alone do not change the intensity of fluorescence. So, when PNBS-CQDs are present with iron (II) ion, by addition of mercury (II) ion, the fluorescence intensity is reduced, and it can be said that the design of a fluorescence probe for mercury (II) ion is logical according to the previous statement.

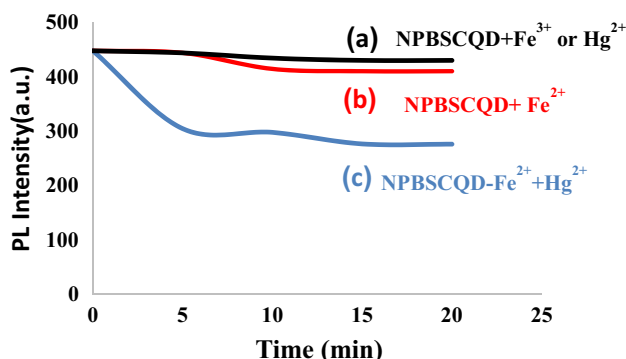


Fig. 3 Fluorescence response of PNBS-CQDs in different times in the presence of Fe²⁺, Fe³⁺, and Hg²⁺ ions and Fe²⁺ + Hg²⁺

3.5 Optimize conditions for detection of Hg²⁺ ion

The parameters to be optimized for mercury ion detection are pH and reaction time. As regards, the reaction of iron (II) ions and mercury (II) ions depends on the pH value, and in view of the fact that, at alkaline pH, metal ions are converted to metal hydroxide form; therefore, for finding optimum value, pH was investigated in the range of 2 to 6 in presence and in the absence of mercury (II) ion. The optimum value for pH is equal to 4. The reaction time is another critical parameter that shows the interaction between PNBS-CQDs, iron (II) ion, and mercury (II) ion. The fluorescence intensity decreases with increasing time and the maximum decrease occurs up to 5 min and after this time the fluorescence intensity did not change. This process of quenching the fluorescence intensity indicates that the reaction described in Eqs. (1) and (2) between mercury and iron (II) ions causes the quenching and the reaction continues up to 5 min.

3.6 Fluorescence determination of Hg²⁺ ion

Under the optimal conditions described above, the fluorescence response of the PNBS-CQDs + Fe²⁺ to different concentrations of mercury (II) is evaluated, and its sensitivity is measured. In Fig. 4a, the fluorescence emission intensity at 530 nm is decreased by increasing the amount of mercury (II) ion. The amount of fluorescence quenching is shown by the ratio of F/F₀ (F₀ and F was the fluorescence intensity of PNBS-CQDs + Fe²⁺ sensing system at 530 nm in the absence and presence of Hg²⁺, respectively) (Fig. 4b). This ratio of F/F₀ has a linear relationship with the concentration of mercury (II) ions in the range of 25 μM to 1500 μM with a correlation coefficient (R²) of 0.99, and according to S/N = 3, the LOD is 5.0 μM and LOQ is 16.5 μM. To better demonstrate the efficiency of this probe in measuring mercury (II) ions, a comparison table with previous work has been reported (Table 1). As it can be seen, the method developed in many aspects including the linear range and detection limit is better than the methods reported so far. Besides, this method is economical and easy to operate, better than other techniques, because there are no dangerous substances and harmful organic substances during the process and its preparation is very convenient [29, 30, 43–45].

3.7 The selectivity of PNBS-CQDs + Fe²⁺ toward different compounds

Selectivity is a significant parameter in evaluating the performance of fluorescence probe. Considering the unique mechanism of PNBS-CQDs + Fe²⁺ in the presence of Hg²⁺, therefore, the selectivity was studied in the presence of other metal ions that may be existing in drinking water, including

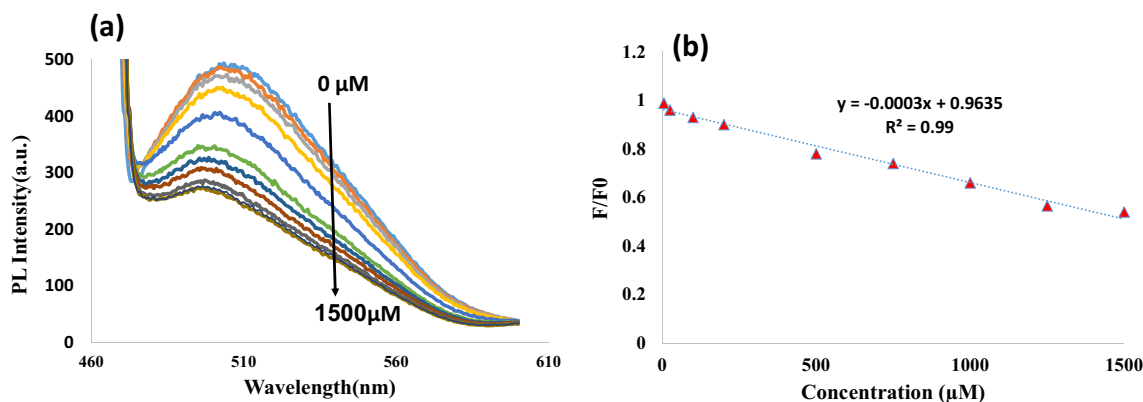


Fig. 4 **a** Fluorescent emission spectra of the PBSN-CQDs + Fe^{2+} upon addition of different concentrations of Hg^{2+} within the range of 25–1500 μM (pH 4), and **b** dependence of F/F_0 on the concentration of Hg^{2+} within the range of 25–1500 μM

Table 1 Comparison of analytical features of Hg^{2+} detection among reported assays

Sr. No	Methods used	Linear range	detection limit	References
1	Nitrogen-doped carbon quantum dots	0–0.1 μM	2.104 nM	[29]
2	Green synthesis of fluorescent carbon nanoparticles	0.5–10 nM	0.23 nM	[30]
3	Carbon nanoparticles	0–5 μM	10 nM	[43]
4	N/S/P-CDs	1–70 μM	1.8×10^{-7} M	[44]
5	Gold nanoprobe	5–100 μM	5 μM	[45]
7	PNBS-CQDs- Fe^{2+}	25–1500 μM	5 μM	This work

silver (I), manganese (II), lead (II), magnesium (II), manganese (II), iron (III), iron (II), cobalt (II), mercury(II), and cadmium (II) 150 μM concentration adding to PNBS-CQDs + Fe^{2+} , and compared the fluorescence intensity with the original fluorescence. It can be seen that fluorescence intensity changes only with the presence of mercury (II) ion that are significant, but for other materials, the fluorescence intensity changes are neglected. This means that PNBS-CQDs + Fe^{2+} are optionally used in an aqueous solution for determination of Hg^{2+} (Fig. 5).

3.8 The quenching effect

Hg^{2+} converts to Hg^0 in the presence of Fe^{2+} , which results in a quenching in the fluorescence intensity of PNBS-CQDs + Fe^{2+} , which can be calculated by the Stern–Volmer Equation: (3)

$$F/F_0 = K_{sv} + [Q] + 1 \quad (3)$$

F_0 and F was the fluorescence intensity of PNBS-CQDs + Fe^{2+} sensing system at 530 nm in the absence and presence of Hg^{2+} , respectively. $[Q]$ is the concentration of Hg^{2+} and K_{sv} is the Stern–Volmer quenching constant, which is related to the quenching efficiency [46,

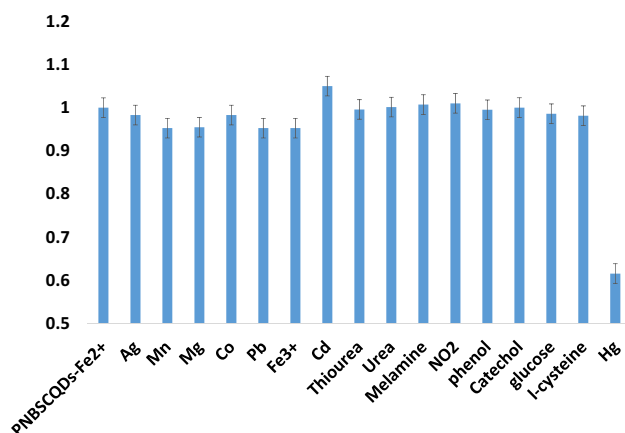


Fig. 5 Fluorescence response of PNBS-CQDs + Fe^{2+} solution toward different metals or biological compounds (excitation at 450 nm; $[M]$ 1000 μM , pH 4)

47]. As shown in Fig. 6, in the range of 25 to 1500 μM , a linear calibration plot between fluorescence intensity change rates $(F_0/F) - 1$ and mercury (II) concentration with a correlation coefficient of $R^2 = 0.97$ is observed. The quenching efficiency (K_{sv}) in the range of 25–1500 μM was $0.6 \times 10^3 \text{ L mol}^{-1}$.

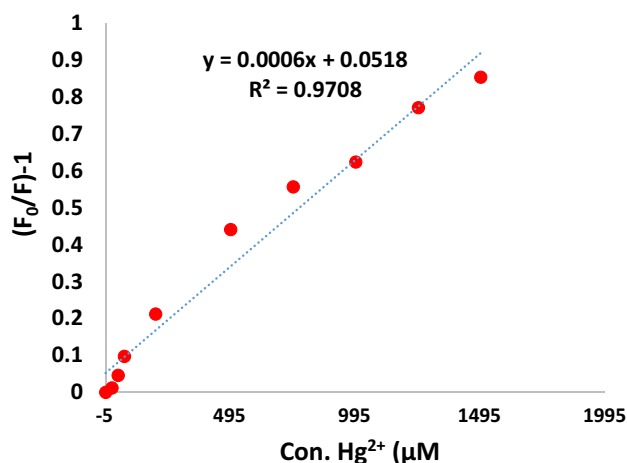
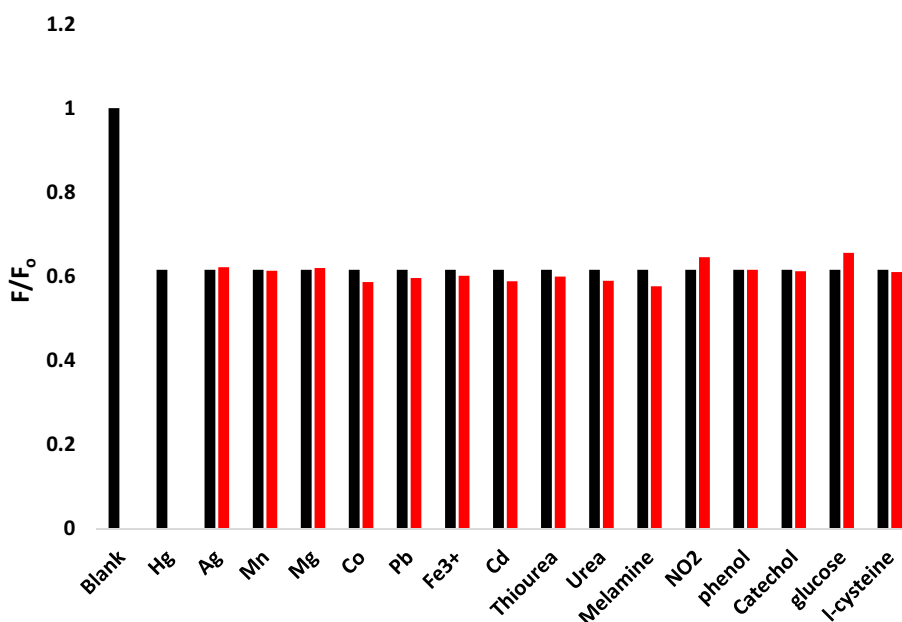


Fig. 6 Stern–Volmer plots representing the quenching effects of Hg²⁺ on the fluorescence emission of CQDs at 4450 nm. The concentration of Hg²⁺ was in the range of 25.0–1500.0 µM

3.9 Interferences

The effects of potential interferences such as metal ions and biochemical compounds on Hg²⁺ (20 µM) detection were investigated. The experimental procedures were as follows: various kinds of interferences were added by firstly testing a 100-fold interference with Hg²⁺; if interference occurred, the concentration of interfering was gradually reduced until the interference ceased. The criterion for interference was that signal change was within 5%. As shown in Fig. 7, the changed fluorescent intensity of PNBS-CQDs + Fe²⁺ probe by 20 µM of Hg²⁺ was not affected by most of the 100-fold excess of ions and biochemical compounds.

Fig. 7 Interference of metal ions and other compounds with Hg²⁺ measurements by PNBS-CQDs + Fe²⁺ probe (pH 4). Blue bars represent the addition of single compounds; red bars represent the mixture of hydrogen peroxide with other compounds



3.10 Detection in real samples

The practical application of the PNBS-CQDs + Fe²⁺ probe in real samples has also been studied. The performance of the PNBS-CQDs + Fe²⁺ fluorescence probe for the detection of Hg²⁺ in real water sample analysis was also investigated by tap water. After the initial preparation of tap water, the mercury ion was determined under optimum conditions (phosphate buffer with pH 4). At first, the water samples were spiked with different concentration of Hg²⁺ and then analyzed with the proposed method (Table 2). Therefore, the probe can be used effectively to analyze mercury (II) ions in the real sample with different matrices.

4 Conclusion

In summary, the water-soluble CDs doped with P, S, B, and N were synthesized for the first time via hydrothermal method. The obtained PNBS-CQDs showed spherical morphology with an average size of 2.5 nm. The PNBS-CQDs + Fe²⁺ and their resultant excitation-independent fluorescence were employed for selective and sensitive detection of Hg²⁺. The as-prepared CDs showed excellent detection capability toward Hg²⁺ over a wide concentration range of 25–1500 µM. It is believed that the fast and selective detection capability for Hg²⁺ by the probe, and also the method developed in many aspects including the linear range and detection limit is better than the methods reported so far. This work would open a new opportunity for the wide application of PNBS-CQDs in the various probe.

Table 2 Determination of concentration amounts of Hg²⁺ in tap water (*n* = 5)

Sample	Added (μM)	Found (μM)	RSD	Recovery (%)
Tap water ^a	10	10.1	3.6	101.0
	20	19.6	4.1	98.0
	50	48.7	3.4	97.4
River water ^b	10	9.8	4.4	98.0
	20	19.2	4.7	96.0
	50	51.2	3.9	102.4

^aKermanshah drinking water, Kermanshah, Iran^bGamasiab river, Kermanshah, Iran

Acknowledgements The authors gratefully acknowledge the Research Council of Kermanshah University of Medical Sciences (Grant Number: 980547) for financial support.

Compliance with ethical standards

Conflict of interest The authors declare that they have no conflict of interest.

References

- M.N. Khan, M.F. Wahab, Characterization of chemically modified corncobs and its application in the removal of metal ions from aqueous solution. *J. Hazard. Mater.* **141**(1), 237–244 (2007)
- A. Renzoni, F. Zino, E. Franchi, Mercury levels along the food chain and risk for exposed populations. *Environ. Res.* **77**(2), 68–72 (1998)
- E.M. Nolan, S.J. Lippard, Tools and tactics for the optical detection of mercuric ion. *Chem. Rev.* **108**(9), 3443–3480 (2008)
- J. Gutknecht, Inorganic mercury (Hg²⁺) transport through lipid bilayer membranes. *J. Membr. Biol.* **61**(1), 61–66 (1981)
- P.B. Tchounwou, W.K. Ayensu, N. Ninashvili, D. Sutton, Environmental exposure to mercury and its toxicopathologic implications for public health. *Environ. Toxicol.* **18**(3), 149–175 (2003)
- S. Zinatloo-Ajabshir, N. Ghasemian, M. Salavati-Niasari, Green synthesis of Ln₂Zr₂O₇ (Ln = Nd, Pr) ceramic nanostructures using extract of green tea via a facile route and their efficient application on propane-selective catalytic reduction of NO_x process. *Ceram. Int.* **46**(1), 66–73 (2020)
- S. Zinatloo-Ajabshir, Z. Salehi, O. Amiri, M. Salavati-Niasari, Simple fabrication of Pr₂Ce₂O₇ nanostructures via a new and eco-friendly route; a potential electrochemical hydrogen storage material. *J. Alloys Compd.* **791**, 792–799 (2019)
- S. Zinatloo-Ajabshir, M. Salavati-Niasari, Preparation of magnetically retrievable CoFe₂O₄@ SiO₂@ Dy₂Ce₂O₇ nanocomposites as novel photocatalyst for highly efficient degradation of organic contaminants. *Compos. B* **174**, 106930 (2019)
- S. Zinatloo-Ajabshir, M.S. Morassaei, M. Salavati-Niasari, Facile synthesis of Nd₂Sn₂O₇-SnO₂ nanostructures by novel and environment-friendly approach for the photodegradation and removal of organic pollutants in water. *J. Environ. Manage.* **233**, 107–119 (2019)
- S. Zinatloo-Ajabshir, M.S. Morassaei, M. Salavati-Niasari, Eco-friendly synthesis of Nd₂Sn₂O₇-based nanostructure materials using grape juice as green fuel as photocatalyst for the degradation of erythrosine. *Compos. B* **167**, 643–653 (2019)
- S. Zinatloo-Ajabshir, M. Salavati-Niasari, A. Sobhani, Z. Zinatloo-Ajabshir, Rare earth zirconate nanostructures: recent development on preparation and photocatalytic applications. *J. Alloys Compd.* **767**, 1164–1185 (2018)
- F. Razi, S. Zinatloo-Ajabshir, M. Salavati-Niasari, Preparation, characterization and photocatalytic properties of Ag₂ZnI₄/AgI nanocomposites via a new simple hydrothermal approach. *J. Mol. Liq.* **225**, 645–651 (2017)
- G. Tz, J. Baasner, M. Gradl, A. Kistner, Determination of mercury in saliva with a flow-injection system. *Anal. Chim. Acta* **320**(2–3), 171–176 (1996)
- H.-T. Wang, B. Kang, T. Chancellor Jr., T. Lele, Y. Tseng, F. Ren, S. Pearton, W. Johnson, P. Rajagopal, J. Roberts, Fast electrical detection of Hg (II) ions with Al Ga N/ Ga N high electron mobility transistors. *Appl. Phys. Lett.* **91**(4), 042114 (2007)
- H. Li, J. Zhai, J. Tian, Y. Luo, X. Sun, Carbon nanoparticle for highly sensitive and selective fluorescent detection of mercury (II) ion in aqueous solution. *Biosens. Bioelectron.* **26**(12), 4656–4660 (2011)
- S. Choi, R.M. Dickson, J. Yu, Developing luminescent silver nanodots for biological applications. *Chem. Soc. Rev.* **41**(5), 1867–1891 (2012)
- X. Michalet, F. Pinaud, L. Bentolila, J. Tsay, S. Doose, J. Li, G. Sundaresan, A. Wu, S. Gambhir, S. Weiss, Quantum dots for live cells, in vivo imaging, and diagnostics. *Science* **307**(5709), 538–544 (2005)
- L. Shang, S. Dong, G.U. Nienhaus, Ultra-small fluorescent metal nanoclusters: synthesis and biological applications. *Nano Today* **6**(4), 401–418 (2011)
- R. Hardman, A toxicologic review of quantum dots: toxicity depends on physicochemical and environmental factors. *Environ. Health Perspect.* **114**(2), 165–172 (2005)
- A.M. Derfus, W.C. Chan, S.N. Bhatia, Probing the cytotoxicity of semiconductor quantum dots. *Nano Lett.* **4**(1), 11–18 (2004)
- S. Tedesco, H. Doyle, J. Blasco, G. Redmond, D. Sheehan, Oxidative stress and toxicity of gold nanoparticles in *Mytilus edulis*. *Aquat. Toxicol.* **100**(2), 178–186 (2010)
- P. Jing, D. Han, D. Li, D. Zhou, D. Shen, G. Xiao, B. Zou, S. Qu, Surface related intrinsic luminescence from carbon nanodots: solvent dependent piezochromism. *Nanoscale Horizons* **4**(1), 175–181 (2019)
- A. Barati, M. Shamsipur, H. Abdollahi, Hemoglobin detection using carbon dots as a fluorescence probe. *Biosens. Bioelectron.* **71**, 470–475 (2015)
- T.T. Bui, S.-Y. Park, A carbon dot-hemoglobin complex-based biosensor for cholesterol detection. *Green Chem.* **18**(15), 4245–4253 (2016)
- S. Dolai, S.K. Bhunia, R. Jelinek, Carbon-dot-aerogel sensor for aromatic volatile organic compounds. *Sens. Actuators B* **241**, 607–613 (2017)
- C. Ding, A. Zhu, Y. Tian, Functional surface engineering of C-dots for fluorescent biosensing and in vivo bioimaging. *Acc. Chem. Res.* **47**(1), 20–30 (2013)
- S.K. Bhunia, S. Dolai, H. Sun, R. Jelinek, “On/off/on” hydrogen-peroxide sensor with hemoglobin-functionalized carbon dots. *Sens. Actuators B* **270**, 223–230 (2018)
- L.S. Walekar, P. Hu, F. Liao, X. Guo, M. Long, Turn-on fluorometric and colorimetric probe for hydrogen peroxide based on the in-situ formation of silver ions from a composite made from N-doped carbon quantum dots and silver nanoparticles. *Microchim. Acta* **185**(1), 31 (2018)

29. W. Lu, X. Qin, S. Liu, G. Chang, Y. Zhang, Y. Luo, A.M. Asiri, A.O. Al-Youbi, X. Sun, Economical, green synthesis of fluorescent carbon nanoparticles and their use as probes for sensitive and selective detection of mercury (II) ions. *Anal. Chem.* **84**(12), 5351–5357 (2012)
30. Y. Tang, L. Rao, Z. Li, H. Lu, C. Yan, S. Yu, X. Ding, B. Yu, Rapid synthesis of highly photoluminescent nitrogen-doped carbon quantum dots via a microreactor with foamy copper for the detection of Hg²⁺ ions. *Sens. Actuators B* **258**, 637–647 (2018)
31. D. Sun, R. Ban, P.-H. Zhang, G.-H. Wu, J.-R. Zhang, J.-J. Zhu, Hair fiber as a precursor for synthesizing of sulfur-and nitrogen-co-doped carbon dots with tunable luminescence properties. *Carbon* **64**, 424–434 (2013)
32. C. Zhao, Y. Jiao, L. Zhang, Y. Yang, One-step synthesis of S, B co-doped carbon dots and their application for selective and sensitive fluorescence detection of diethylstilbestrol. *New J. Chem.* **42**(4), 2857–2864 (2018)
33. X. Gong, Q. Zhang, Y. Gao, S. Shuang, M.M. Choi, C. Dong, Phosphorus and nitrogen dual-doped hollow carbon dot as a nanocarrier for doxorubicin delivery and biological imaging. *ACS Appl. Mater. Interfaces* **8**(18), 11288–11297 (2016)
34. X. Gong, Q. Hu, M.C. Paau, Y. Zhang, S. Shuang, C. Dong, M.M. Choi, Red-green-blue fluorescent hollow carbon nanoparticles isolated from chromatographic fractions for cellular imaging. *Nanoscale* **6**(14), 8162–8170 (2014)
35. X. Jin, X. Sun, G. Chen, L. Ding, Y. Li, Z. Liu, Z. Wang, W. Pan, C. Hu, J. Wang, pH-sensitive carbon dots for the visualization of regulation of intracellular pH inside living pathogenic fungal cells. *Carbon* **81**, 388–395 (2015)
36. R. Qian, L. Ding, L. Bao, S. He, H. Ju, In situ electrochemical assay of cell surface sialic acids featuring highly efficient chemoselective recognition and a dual-functionalized nanohorn probe. *Chem. Commun.* **48**(32), 3848–3850 (2012)
37. X. Gong, Y. Liu, Z. Yang, S. Shuang, Z. Zhang, C. Dong, An “on-off-on” fluorescent nanoprobe for recognition of chromium (VI) and ascorbic acid based on phosphorus/nitrogen dual-doped carbon quantum dot. *Anal. Chim. Acta* **968**, 85–96 (2017)
38. X. Gong, W. Lu, M.C. Paau, Q. Hu, X. Wu, S. Shuang, C. Dong, M.M. Choi, Facile synthesis of nitrogen-doped carbon dots for Fe³⁺ sensing and cellular imaging. *Anal. Chim. Acta* **861**, 74–84 (2015)
39. L. Ji, L. Chen, P. Wu, D.F. Gervasio, C. Cai, Highly selective fluorescence determination of the hematin level in human erythrocytes with no need for separation from bulk hemoglobin. *Anal. Chem.* **88**(7), 3935–3944 (2016)
40. V.K. Singh, P.K. Yadav, S. Chandra, D. Bano, M. Talat, S.H. Hasan, Peroxidase mimetic activity of fluorescent NS-carbon quantum dots and their application in colorimetric detection of H₂O₂ and glutathione in human blood serum. *Journal of Materials Chemistry B* **6**(32), 5256–5268 (2018)
41. A. Barati, M. Shamsipur, H. Abdollahi, Carbon dots with strong excitation-dependent fluorescence changes towards pH. Application as nanosensors for a broad range of pH. *Anal. Chim. Acta* **931**, 25–33 (2016)
42. R.R. Raposo, E. Meléndez-Hevia, M. Spiro, Autocatalytic formation of colloidal mercury in the redox reaction between Hg²⁺ and Fe²⁺ and between Hg₂²⁺ and Fe²⁺. *J. Mol. Catal. A* **164**(1–2), 49–59 (2000)
43. Y. Guo, Z. Wang, H. Shao, X. Jiang, Hydrothermal synthesis of highly fluorescent carbon nanoparticles from sodium citrate and their use for the detection of mercury ions. *Carbon* **52**, 583–589 (2013)
44. C. Wang, D. Sun, K. Zhuo, H. Zhang, J. Wang, Simple and green synthesis of nitrogen-, sulfur-, and phosphorus-co-doped carbon dots with tunable luminescence properties and sensing application. *RSC Adv.* **4**(96), 54060–54065 (2014)
45. S. He, D. Li, C. Zhu, S. Song, L. Wang, Y. Long, C. Fan, Design of a gold nanoprobe for rapid and portable mercury detection with the naked eye. *Chem. Commun.* **40**, 4885–4887 (2008)
46. F. Coppin, J. Michon, C. Garnier, S. Frelon, Fluorescence quenching determination of uranium (VI) binding properties by two functional proteins: Acetylcholinesterase (AChE) and vitellogenin (Vtg). *J. Fluorescence* **25**(3), 569–576 (2015)
47. Y. Liu, H. Xue, J. Liu, Q. Wang, L. Wang, Carbon quantum dot-based fluorometric nitrite assay by exploiting the oxidation of iron (II) to iron (III). *Microchim. Acta* **185**(2), 129 (2018)

Publisher's Note Springer Nature remains neutral with regard to jurisdictional claims in published maps and institutional affiliations.